 doi:10.20944/preprints202210.0269.v1

Article

Micro-Scale Flow Excitation under Imposition of Uniform Magnetic Field and Electrical Current

Guangye Xu [1,*] and Kazuhiko Iwai [1]

[1] Faculty of Engineering, Hokkaido University, Kita 13 Nishi 8 Kita-ku, Sapporo, Hokkaido, 060-8628, Japan; xuguangye@eis.hokudai.ac.jp

* Correspondence: xuguangye@eis.hokudai.ac.jp

Abstract: Mass transfer is often the rate determining step for solid-liquid chemical reactions. Decrease of the concentration boundary layer thickness is essential to intensify the chemical reaction. Because the concentration boundary layer exists in the velocity boundary layer, force imposition in the concentration boundary layer by superimposing an electrical current and a magnetic field was proposed. Through, flow can be directly excited in the concentration boundary layer. The previous result indicates that by superimposing a DC current and a gradient magnetic field, the development of the concentration boundary layer was suppressed, because of a macro-scale flow excitation in the whole vessel. And by superimposing the gradient magnetic field with a modulate current, the development of the concentration boundary layer was further suppressed. This is because of the macro-scale flow enhancement and the excitation of a micro-scale flow near the solid-liquid interface. However, the mechanism for the micro-scale flow excitation has not been clarified. To clarify this, a uniform magnetic field was superimposed with the DC current or the modulate current. By this means, only the micro-scale flow was excited near the anode surface. The results found that the non-unform electromagnetic force distribution is the main reason for the micro-scale flow excitation.

Keywords: mass transfer; micro-scale flow; diffusion; convection

1. Introduction

The enhancement of solid-liquid chemical reaction rate is important for the time and energy saving. For solid-liquid chemical reactions, mass transfer is often the rate determining step. For instance, a refining process in the metallurgy industry and an electroplating process in the aerospace industry [1-4]. To enhance the solid-liquid chemical reaction rate, the enhancement of mass transfer in a concentration boundary formed near the solid-liquid interface is important.

The mass transfer in the concentration boundary layer is dependent on the diffusion and the convection [5, 6]. Fick's first law indicates that the intensity of the former part positively relates to the diffusion coefficient and the concentration gradient [7]. The enhancement of mass transfer by intensifying the diffusion coefficient is difficult, because the diffusion coefficient is one of the physical properties of the liquid. This means that the intensification of the concentration gradient near the solid-liquid interface is effective for the enhancement of the mass transfer. On the other hand, the convection contributes to enhance the mass transfer, because it increases the concentration gradient by decreasing the concentration boundary layer thickness [6]. Thus, traditional methods like mechanical agitation excite a flow in the bulk region to enhance the solid-liquid chemical reaction rate [8-10].

By exciting the flow in the bulk region, a velocity boundary layer forms in the vicinity of the solid-liquid interface. The velocity in it increases form zero velocity at the interface to a maximum in the mainstream of flow [11,12]. The relative thickness between the velocity boundary layer and the concentration boundary layer is a function of Schmidt number as shown in the following equation [13]:

Preprints (www.preprints.org) | NOT PEER-REVIEWED | Posted: 19 October 2022 doi:10.20944/preprints202210.0269.v1

$$Sc = \frac{\upsilon}{D} \tag{1}$$

Here, υ is the kinematic viscosity and D is the diffusion coefficient.

For liquids, the Schmidt number is usually much larger than unity [14]. Thus, the concentration boundary layer is in the velocity boundary layer, and the traditional methods decrease the concentration boundary layer from its outside. These mean that the flow in the concentration boundary layer is limited, and a strong agitation in the bulk region is required to enhance the mass transfer. The excessive agitation in the bulk region also results in some problems. For instance, the injury of the vessel.

Because the concentration boundary layer exists in the velocity boundary layer, a direct force imposition in the concentration boundary layer is a promising way to enhance mass transfer. Through this, a direct flow excitation in the concentration boundary layer is expected, which enhances the mass transfer in the concentration boundary layer by convection. Based on this concept, a new method of exciting flow in the concentration boundary layer by imposing an electromagnetic force was proposed [15-17]. Because the force is imposed by superimposing an electrical current and a magnetic field, the application of this method on industrial process dealing with a conductive liquid is expected [18, 19]. Compared to the traditional methods, force can be directly imposed near the solid-liquid interface without physical contact. Therefore, the problems caused by the excessive bulk liquid agitation and the contamination of the liquid phase due to the wear or corrosion of the agitator can be prevented.

In the previous study [16], Yokota et.al evaluated the Cu^{2+} concentration time variation in a Cu^{2+} concentration boundary layer with high Cu^{2+} concentration formed by dissolving a Cu anodic electrode into a Cu^{2+} electrolyte solution. They found that by imposing a DC current with a gradient magnetic field, the development of the concentration boundary layer was suppressed compared to that with only the DC current imposition. And by superimposing the gradient magnetic field and a modulate current composed of the DC current and an AC current, the development of the concentration boundary layer was further suppressed. The same phenomena were also observed in the whole vicinity of the anode surface [17]. These are because that by superimposing the gradient magnetic field with the current, the difference in the intensities of the electromagnetic force near the anode and near the cathode led to the excitation of a macro-scale flow in the whole vessel. By this means, liquid with initial Cu^{2+} concentration flowed from the bulk region to the vicinity of the anode surface, which suppressed the increase of the Cu^{2+} concentration. And by imposing the gradient magnetic field with the modulate current, the development of the macro-scale flow was enhanced, and a micro-scale flow was excited near the anode surface. However, the mechanism for the micro-scale flow excitation has not been clarified. To clarify this, a uniform magnetic field was superimposed with the electrical current. Because the electromagnetic force difference between near the anode and near the cathode was suppressed, the suppression of the macro-scale flow excitation and the excitation of only the micro-scale flow are expected.

2. Experimental Methods

Figure 1 indicates the bird-eye view of the experimental apparatus. A transparent vessel was filled by a 0.3 mol/L $CuSO_4$ + 0.1 mol/L H_2SO_4 aqueous solution. The inner length and the inner depth of the vessel is 20 mm and 4 mm, respectively. A Cu anodic electrode and a Cu cathodic electrode were set in the lower and upper parts of the vessel, respectively. And the left and right sides of the lower part electrode were covered by 5 mm length insulators. Fig. 1 also shows the definition of the coordinate system in this study. Its origin is defined as the center of the anode. The horizontal, vertical, and depth directions were indicated by the x-axis, y-axis, and z-axis, respectively.

Preprints (www.preprints.org) | NOT PEER-REVIEWED | Posted: 19 October 2022 doi:10.20944/preprints202210.0269.v1

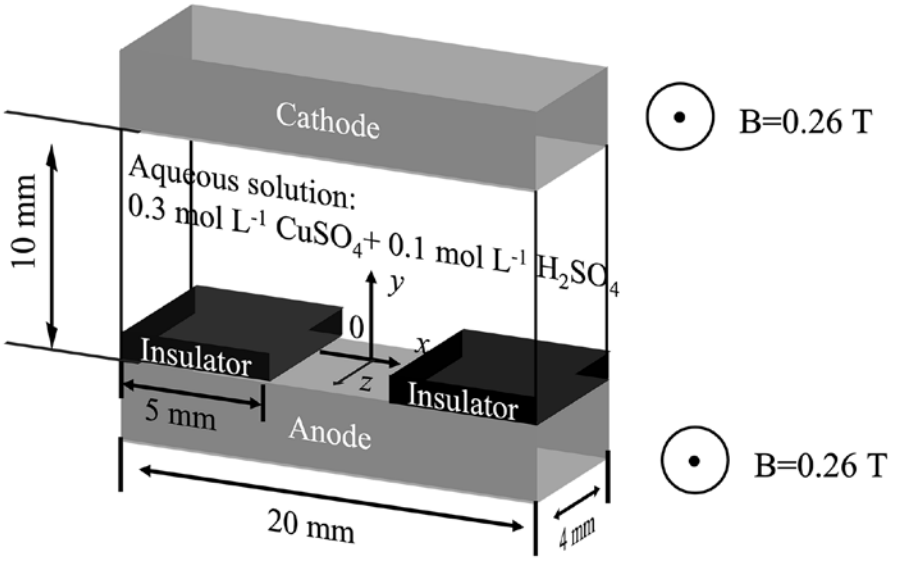

Figure 1. Bird-eye view of experimental apparatus.

The five experimental conditions with their abbreviations are shown in Table 1. Four current conditions were used in this study. One was a 25 mA DC current. The others are modulate currents of the superimposition of the 25 mA DC current and a 2 Hz, 30 mAp-p or a 6 Hz, 30 mAp-p AC current, and the superimposition of the 25 mA DC current and a 2 Hz, 50 mAp-p AC current. The average current intensities of these four current conditions were 25 mA. The experimental condition of only the 25 mA DC current imposition was expressed as the 'DC condition'. The experimental condition of the superimposition of the DC current and a uniform magnetic field is expressed as the 'DC+MF' condition. The uniform magnetic field was in the negative z-direction, and its intensities near the anode and near the cathode were the same of 0.26 T. The experimental conditions of the simultaneous imposition of the uniform magnetic field and the 2 Hz, 30 mAp-p, the 6 Hz, 30 mAp-p, or the 2 Hz, 50 mAp-p modulate current was expressed as the '2 Hz, 30 mA condition', the '6 Hz, 30 mA condition' or the '2 Hz, 50 mA condition', respectively.

Table 1. Experimental conditions

	Experimental condition abbreviation	DC current intensity (mA)	AC current amplitude (mA)	AC current frequency (Hz)	Magnetic field intensity near anode (T)	Magnetic field intensity near anode (T)
1	DC condition	25	0	none	0	0
2	DC+MF condition	25	0	none	0.26	0.26
3	2 Hz, 30 mA condition	25	30	2	0.26	0.26
4	6 Hz, 30 mA condition	25	30	6	0.26	0.26
5	2 Hz, 50 mA condition	25	50	2	0.26	0.26

Because of the current imposition, the Cu anodic electrode dissolved into the Cu^{2+} aqueous solution. By this means, a Cu^{2+} concentration boundary layer with higher Cu^{2+} concentration compared to that of the bulk liquid formed near the anode surface. Based on the Lambert-Beer's law [20,21], the brightness of the Cu^{2+} aqueous solution decreases with the increase of Cu^{2+} concentration. And the Cu^{2+} concentration can be evaluated by measuring the liquid brightness based on the following equation.

Preprints (www.preprints.org) | NOT PEER-REVIEWED | Posted: 19 October 2022 doi:10.20944/preprints202210.0269.v1

$$c = \frac{\log_{10}\left(\frac{I_1}{I_2}\right)}{-\epsilon l} + A \quad (2)$$

where A is a constant, c is the Cu^{2+} concentration, I_1 is the brightness of objective liquid, I_2 is the brightness of a standard liquid, l is the optical path length, and ϵ is the molar absorption coefficient, respectively.

The time variation and the non-uniform distribution of natural light intensity might lead to the experimental errors on the brightness measurement results. To exclude these experimental errors, the experiments were conducted in a dark curtain, with a flat light source set at the back of the vessel for a uniform light incident. The brightness of the aqueous solution was recorded by a video recorder set in front of the vessel with a frame rate of 50 frames per second and a pixel size of 40 μm × 40 μm. Because the shape of the vessel was symmetric, the brightness was measured in the x-range of -1 mm to 5 mm. The vertical distance between the brightness measurement position and the right end of the anode surface with the y-range of 160 μm to 200 μm.

The velocity of the liquid was measured in the y-range of 120 μm- 280 μm by using polystyrene particles with a diameter of 80μm. The measurement method was similar with the previous research [15-17].

3. Results and discussion

3.1. Concentration measurement results

Figure 2(a) shows the measured Cu^{2+} concentration distribution results under the DC condition. The average Cu^{2+} concentration in the x-ranges of from -1 mm to 1 mm, from 1 mm to 3 mm and from 3 mm to 5 mm was measured. For an expression convenience, these x-ranges were named as the x-positions of 0 mm, 2 mm and 4 mm, respectively. The Cu^{2+} concentration increased with increasing the x-position. And this corresponds to the previous results [17]. Because of the surface area difference between the cathode and the anode, current concentration occurred near the right end of the anode surface. That is, the current intensity near the right part was larger than that near the middle part. In addition, the concentration difference between at 4 mm and at 2 mm or at 0 mm increased with time. Because of the positive relation between the electrical conductivity and the Cu^{2+} concentration [23,24], the current intensity difference between at 4 mm and at 2 mm or at 0 mm was enhanced. The Cu^{2+} concentration at 5 s was the minus value at 0 mm. This might be caused by the irregular light reflection on the uneven anode surface, which might result in the slight increase or decrease in the measurement concentration compared to the actual concentration. On the other hand, the irregular light reflection might be suppressed at the right end due to the relatively dark liquid solution. Because of the relatively large concentration difference of more that 0.02 mol/L between at 4 mm and 2 mm or 0 mm from 5 s, it is considered that the higher Cu^{2+} concentration at 4 mm compared to that at 0 mm and 2 mm is not caused by the experimental error.

Figure 2(b) shows the comparison between the average Cu^{2+} concentration measurement results in the x-range of from -1 mm to 5 mm and the theoretical Cu^{2+} concentration under the DC condition. The theoretical Cu^{2+} concentration was calculated at the y-positions of 160 μm and 200 μm. For the theoretical Cu^{2+} concentration calculation, the diffusion phenomenon was simplified as a one-dimensional model in positive y-direction. And the boundary condition and the dissolved Cu^{2+} concentration near the anode surface when imposing a current from 0 s is shown in the following equations [25]:

$$c_{(y=0,t=0)} = c_0 \quad (3)$$

$$c_{(y=\infty,t=t)} = c_0 \quad (4)$$

Preprints (www.preprints.org) | NOT PEER-REVIEWED | Posted: 19 October 2022 doi:10.20944/preprints202210.0269.v1

$$2FD\left(\frac{\partial c}{\partial y}\right)_{y=0} = J \tag{5}$$

$$c_{y,t} - c_{y,0} = \frac{J}{2FD} \times \left[2\sqrt{\frac{Dt}{\pi}}exp\left(-\frac{y^2}{4Dt}\right) - yerfc\left(\frac{y}{2\sqrt{Dt}}\right)\right] \tag{6}$$

Here, c_0 is the initial concentration, D=5.5 × 10^{-10} m²/s [26, 27] is the Cu^{2+} diffusion coefficient, F is the Faraday's constant, J is the current density, t is the time, and y is the vertical position respectively.

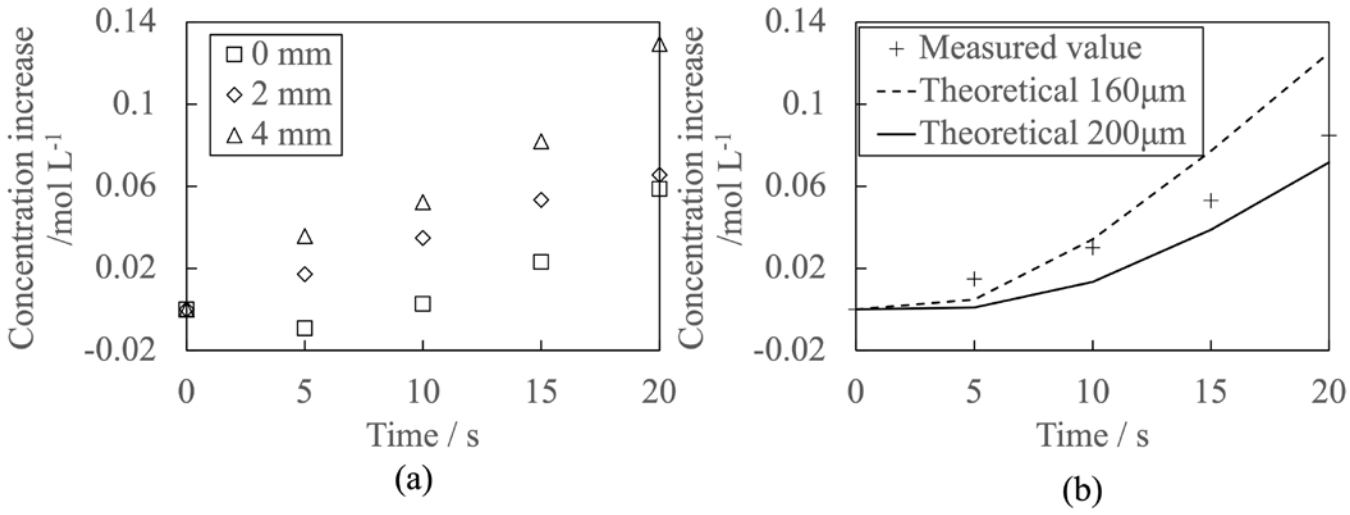

Figure 2. (**a**) Concentration distribution and (**b**) comparison between the theoretical Cu^{2+} concentration at 160 μm, 200 μm and measured Cu^{2+} concentration under DC condition in y-range of 160 μm-200μm

The measured average concentration at 5 s was larger than the theoretical value at 160 μm and 200 μm. The reason might be caused by the experimental error due to the irregular light reflection on the uneven anode surface as mentioned above. And it is considered that this experimental error was suppressed with time because the liquid brightness near the anode surface decreased with time, which contributes to suppress the light reflection on the uneven anode surface. The measured average concentration from 10 s to 20 s was between the theoretical concentration calculation results at 160 μm and 200 μm. This is because the measured concentration was the average concentration in one pixel with the height of 40 μm. The concentration difference between the measured value and the theoretical value at 160 μm increased, and between the measured value and the theoretical value at 200 μm decreased from 10 s to 20 s. This is contributed to the inverse relationship between the Cu^{2+} concentration and the Cu^{2+} diffusion coefficient [23,24]

3.2. Velocity measurement results and liquid flow pattern observation results

Flow was not excited under the DC condition. Because of the uniform magnetic field imposition, electromagnetic force intensity difference between near the anode and near the cathode was suppressed. Consequently, the macro-scale flow in the whole vessel was not observed, and only a micro-scale flow was excited near the anode surface. Fig. 3 shows the maximum velocity and the minimum velocity measurement results under the DC+MF condition. The maximum velocity and the absolute value of the minimum velocity are

Preprints (www.preprints.org) | NOT PEER-REVIEWED | Posted: 19 October 2022 doi:10.20944/preprints202210.0269.v1

very close. In addition, the magnitudes of the maximum velocity and the absolute value of the minimum velocity increased with time. This indicates the development of the flow.

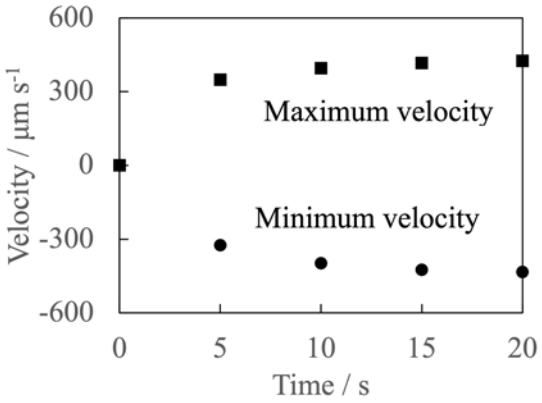

Figure 3. Velocity measurement results under DC+MF condition.

Because the magnitudes of the maximum velocity and the absolute value of the minimum velocity were essentially the same under the experimental conditions with the superimposition of current and magnetic field, only the maximum velocity measurement results under these experimental conditions were shown in Fig. 4. The maximum velocity under the experimental conditions with the AC current imposition was larger than that under the DC+MF condition. This means that by adding the AC current, the micro-scale flow excitation was enhanced. The higher maximum velocity under the 2 Hz, 30 mA condition compared to that under the 6 Hz, 30 mA condition indicates that by decreasing the AC current frequency, the micro-scale flow development was enhanced. On the other hand, the maximum velocity under the 2 Hz, 50 mA condition was larger than that under the 2 Hz, 30 mA condition. And its value was the largest among the four experimental conditions shown in Fig. 3. These mean that by increasing the AC current amplitude, the micro-scale flow development was further enhanced.

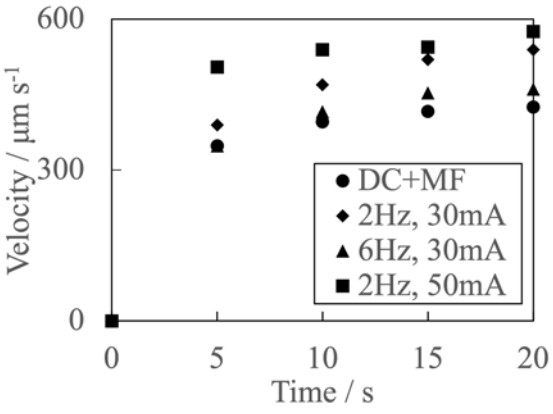

Figure 4. Maximum velocity measurement results.

The liquid flow pattern under the DC+MF condition is shown in Fig. 5. The micro-scale flow essentially parallel to the anode surface was observed just above the anode surface. The flow in the center of the depth direction was in the positive x-direction. And near the front and back walls, the flow was in the negative x-direction.

Preprints (www.preprints.org) | NOT PEER-REVIEWED | Posted: 19 October 2022 doi:10.20944/preprints202210.0269.v1

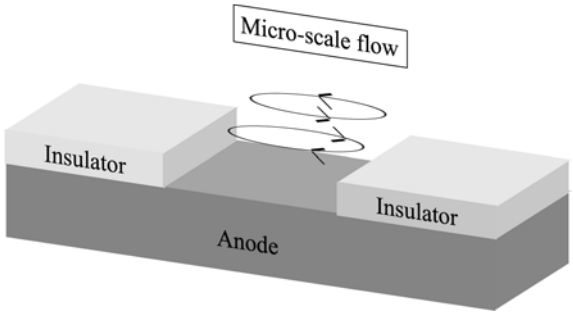

Figure 5. Liquid flow pattern under DC+MF condition from 5 s to 20 s in the *y*-range of 120 μm to 280 μm.

Figure 6 shows the liquid flow patterns under the 2 Hz, 30 mA condition and the 6 Hz, 30mA condition. The liquid flow pattern under these two conditions were essentially the same within 20 s, and the flow region extended with time. The micro-scale flow was observed just above the anode surface at the initial stage, as shown in Fig. 6(a). It firstly extended above the upper part of the left side insulator as shown in Fig. 6(b), and it extended above the upper part of the right side insulator at around 20 s as shown in Fig. 6(c). The reason for the essentially same flow region under these two conditions though the maximum velocity under the 2 Hz, 30 mA condition was larger than that under the 6 Hz, 30 mA condition might because of the limitation of the experimental time.

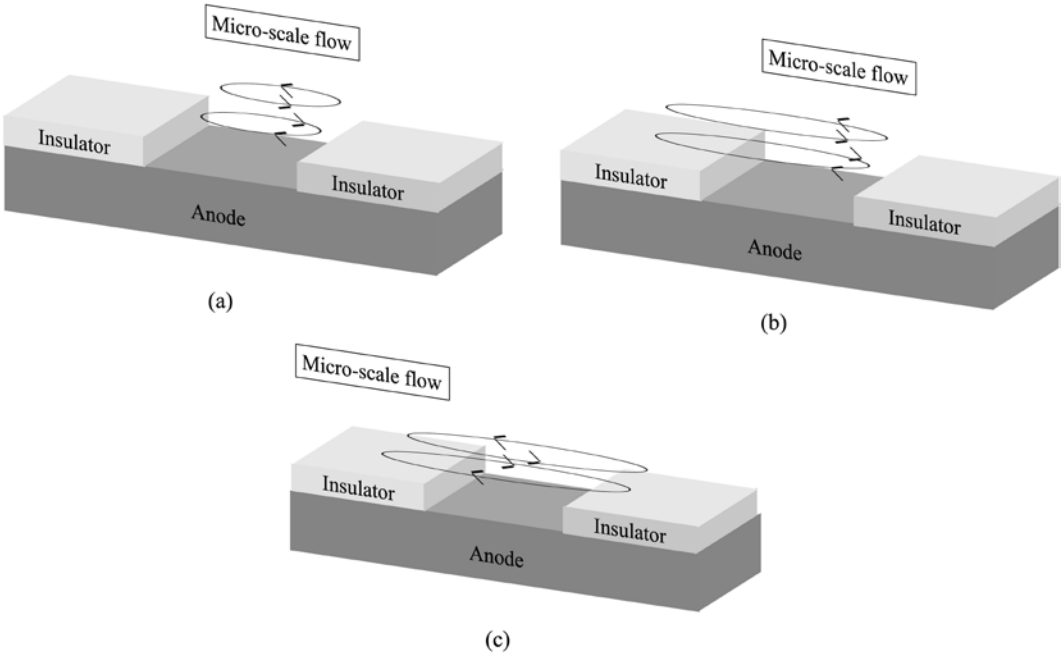

Figure 6. Liquid flow pattern under 2 Hz, 30 mA and 6 Hz, 30 mA conditions (**a**) at initial stage, and (**b**) and (**c**) with time development in the *y*-range of 120 μm to 280 μm.

The liquid flow pattern under the 2 Hz, 50 mA condition was different from those under the DC+MF condition, the 2 Hz, 30 mA condition, and the 6 Hz, 30 mA condition, as shown in Fig. 7. The micro-scale flow was observed not only just above the anode surface, but also above the left and right sides insulators from the initial stage.

Preprints (www.preprints.org) | NOT PEER-REVIEWED | Posted: 19 October 2022 doi:10.20944/preprints202210.0269.v1

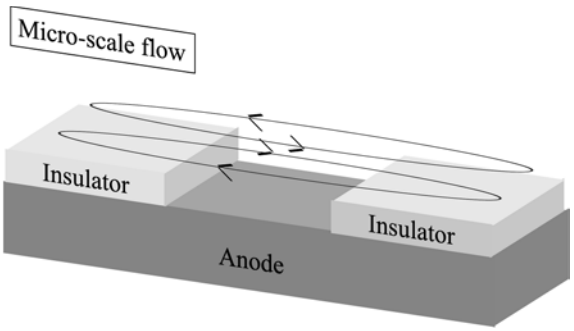

Figure 7. Liquid flow pattern under 2 Hz, 50 mA condition from 5 s to 20 s in the y-range of 120 μm to 280 μm.

Figure 8 shows the mechanism of the micro-scale flow excitation. Because the surface area of the cathode was two times larger than that of the anode, the current concentration took place near the side parts of the anode surface [22]. And the current directions near the left and right parts of the anode surface were not perpendicular to the anode surface, as shown by the dashed arrows in Fig. 8(a). Thus, the electromagnetic force directions were oblique upward, parallel and oblique downward to the anode surface near the left, middle and right parts respectively. Near the left part of the anode surface, the upward electromagnetic force component led to an upward motion of liquid with high Cu^{2+} concentration around the center in the depth direction, because the upward liquid motion near the side walls was suppressed due to the friction, as shown in Fig. 8(b). Therefore, the non-uniform Cu^{2+} concentration distribution took place in the depth direction, in which the Cu^{2+} concentration near the side walls was smaller than that in the center of the vessel, as shown in Fig. 8(c). Because of the positive relationship between the Cu^{2+} concentration and the electrical conductivity [23, 24], the horizontal electromagnetic force component intensity around the center of the depth direction was larger than that near the side walls as shown in Fig. 8(d), and this force difference increased with time. The electromagnetic force difference in the depth direction is the driving force of the micro-scale flow excitation. Because of the larger horizontal electromagnetic force component in the center of the depth direction, the micro-scale flow direction in the center was the positive x-direction and near the side walls was the negative x-direction. On the other hand, the maximum current intensity under the experimental conditions with the superimposition of the modulate current and the uniform magnetic field was larger than that under the DC+MF condition. This means that the driving force for the micro-scale flow excitation was enhanced by adding the AC current. Thus, the extension of the micro-scale flow region and the higher maximum velocity were observed under the experimental conditions with the superimposition of the modulate current and the uniform magnetic field in comparison to that under the DC+MF condition. Because the micro-scale flow originated from the left part of the anode surface, time for the flow region to extend above the upper part of the left side insulator was shorter than that to the right side insulator. However, the reason for the increase of the AC current frequency led to the decrease of the maximum velocity was not clarified. And this will be investigated in the future work. In addition, by increasing the AC current amplitude, the driving force for the micro-scale flow was further enhanced. Thus, the micro-scale flow under the 2 Hz, 50 mA condition was observed not only just above the anode surface, but also above the upper part of the insulators from the initial stage, and the maximum velocity under the 2 Hz, 50 mA condition was larger than those under the DC+MF condition, the 2 Hz, 30 mA condition and the 6 Hz, 30 mA condition.

Preprints (www.preprints.org) | NOT PEER-REVIEWED | Posted: 19 October 2022 doi:10.20944/preprints202210.0269.v1

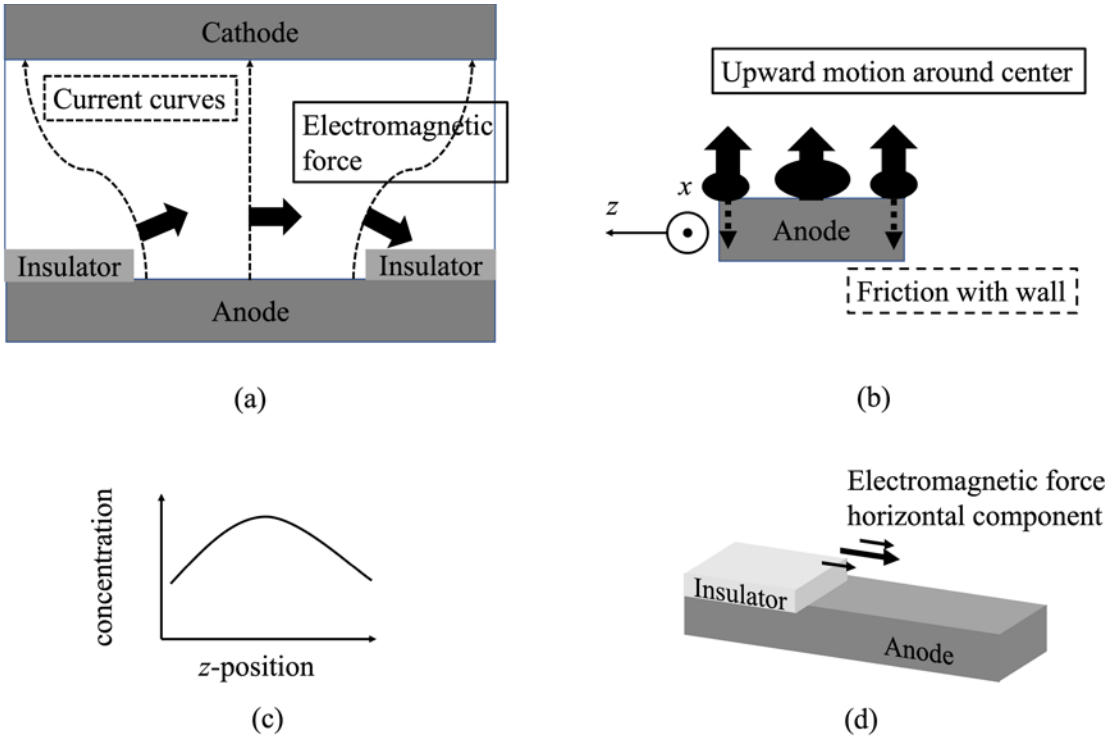

Figure 8. Schematics of (**a**) current and electromagnetic force distributions, (**b**) right side view of upward liquid motion near the left side, (**c**) concentration distribution in *z*-direction and (**d**) electromagnetic force horizontal component distribution near left part.

4. Conclusions

To study the mechanism for the micro-scale flow excitation, a uniform magnetic was superimposed with an electrical current. And the following results were obtained:

1. By superimposing the current and the uniform magnetic field, micro-scale flow parallel to the anode surface was observed. The reason for the micro-scale flow excitation is because of the non-uniform electromagnetic force distribution.
2. By superimposing the modulate current with the uniform magnetic field, flow region was extended, and the maximum velocity increased compared to that under the superimposition of the DC current and the magnetic field. This is because the driving force for the micro-scale flow excitation was enhanced.
3. The decrease of the AC current frequency led to an increase of the maximum velocity. However, the obvious influence of the AC current frequency on the liquid flow pattern was not observed within 20 s.
4. By increasing the AC current amplitude, the largest maximum velocity and the extension of the flow region compared to those under the DC+MF condition, the 2 Hz, 30 mA condition and the 6 Hz, 30 mA condition were observed from the initial stage.

Author Contributions: Conceptualization, K. Y.; methodology, G.X.; validation, G.X. and K.I.; formal analysis, G.X. and K.I.; investigation, G.X.; resources, K.I.; data curation, G.X.; writing—original draft preparation, G.X.; writing—review and editing, K.I.; visualization, G.X. and K.I.; supervision, K.I.; project administration, K.I.; funding acquisition, K.I. All authors have read and agreed to the published version of the manuscript.

Data Availability Statement: The data used to support the findings of this study are available from the corresponding author upon request.

Acknowledgments: The first author gratefully acknowledges the financial support from China Scholarship Council (No. 201806060147), which has sponsored his study at the Hokkaido University in Japan.

Conflicts of Interest: The authors declare no conflict of interest.

References

1. Wen, C. Y. Noncatalytic heterogeneous solid-fluid reaction models. *J. Ind. Eng. Chem.* **1968**, *60*, 34-54
2. Iwai, K.; Yokota, T.; Maruyama, A.; Yamada, T. Oscillating Electromagnetic Force Effect on Concentration Distribution near Liquid Solid Interface. *IOP Conf. Ser.: Mater. Sci. Eng.* **2018**, *424*, 012051.
3. Frank, C. W. The Kinetics of Electrode Reactions: Part II—mass transfer and mixed control. *J. Ind. Eng. Chem.* 1992, *70*, 95-99.
4. Madden, J. D.; Hunter, I. W. Three-dimensional microfabrication by localized electrochemical deposition. *J. Microelectromech. Sys.* **1996**, *5*, 24-32.
5. Jaiswal, D. K; Kumar, A.; Yadav, R. R. Analytical Solution to the One-Dimensional Advection-Diffusion Equation with Temporally Dependent Coefficients. *J. Water Resource Prot.* **2011**, *3*, 76-84.
6. Stocker, T. *Introduction to Climate Modelling*, 1st ed.; Springer: Berlin, Germany, 2011; pp. 57.
7. Bird, R. B.; Stewart, W. E.; Lightfoot, E. N. *Transport Phenomena,* 2nd ed.; John Wiley and Sons: New York, the United States of America, 2007; pp. 621.
8. Umezawa, K.; Matsunaga, H., Tonomura, R.; Furugaki, I. The influence of operating condition on dephosphorization and desulphurization reactions of hot metal with lime-based flux. *Tetsu-to-Hagane*, **1983**, *15*, 1810-1817.
9. Panneerselvam, R.; Savithri, S.; Surender, G. D. CFD modeling of gas–liquid–solid mechanically agitated contactor. *Chem. Eng. Res. Des.* **2008**, *86*, 1331-1344.
10. Ilegbusi, O. J. The role of gas plumes in agitation and mass transfer in metallurgical systems. *Steel Res.* **1994**, *65*, 534-540.
11. Rohsenow, W. M.; Choi, H. Y. *Heat, Mass and Momentum Transfer*, 1st ed.; Prentice-Hall, Inc.: New Jersey, the United States of America, 1963; pp. 25.
12. Streeter, V. L. *Fluid Mechanics*, 2nd ed.; McGRAW- Hill Book Company, Inc.: New York, the United States of America, 1958; pp. 3.
13. Welty, J. R.; Wicks, C. E.; Wilson, R. E.; Rorrer, G. L. *Fundamentals of Momentum, Heat, and Mass Transfer,* 5th ed.; John Wiley & Sons, Inc.: New Jersey, the United State of America, 2000; pp. 519.
14. Gualtieri, C.; Angeloudis, A.; Bombardelli, F.; Jha, S.; Stoesser, T. On the Values for the Turbulent Schmidt Number in Environmental Flows. *Fluids* **2017**, *2*, 17.
15. Yokota, T.; Maruyama, A.; Yamada, T.; Iwai, K. Direct observation of concentration boundary layer formed in the vicinity of anode electrode under imposition of vibrating electromagnetic force. *Tetsu-to-Hagane* **2016**, *102*, 119-126.
16. Yokota, T.; Maruyama, A.; Yamada, T.; Iwai, K. Decrease of concentration boundary layer thickness by using vibrating electromagnetic force. *J. Japan. Inst. Met. Mater.* **2017**, *81*, 516-521.
17. Xu, G.; Iwai, K. Solute concentration distribution in the vicinity of solid-liquid interface under the imposition of a time-varying force. *ISIJ Int.* **2022**, *62*, 1389-1395.
18. Moon, K. H.; Shin, H. K.; Kin, B. J.; Chung, J. Y.; Hwang, Y. S.; Yoon, J. K. Flow control of molten steel by electromagnetic brake in the continuous casting mold. *ISIJ Int.* **1996**, *36*, S201-S203.
19. Moffatt, H. K. Electromagnetic stirring. *Phys. Fluids A.* **1991**, *3*, 1336-1343.
20. Swinehart, D. F. The Beer-Lambert law, *J. Chem. Educ.* **1962**, *39*, 333.
21. Mayerhöfer, T. G.; Mutschke, H.; Popp, J. Employing theories far beyond their limits—the case of the (Boguer-) beer–lambert law. *ChemPhysChem.* **2016**, *17*, 1948-1955.
22. Kanani, N. *Electroplating- Basic Principles, Processes and Practice,* 1st ed.; Elsevier: Amsterdam, the Netherlands, 2005; pp. 99-105.
23. Price, D. C; Davenport, W. G. Densities, electrical conductivities and viscosities of $CuSO_4/H_2SO_4$ solutions in the range of modern electrorefining and electrowinning electrolytes. *Metall. Mater. Trans. B* **1980**, *11*, 159-163.
24. The Chemical Society of Japan. *Handbook of Chemistry, Basics II,* 3rd ed.; Maruzen: Tokyo, Japan, 1984; pp. 453.
25. Fueki, K. *Handbook of electrochemistry,* 4th ed.; Maruzen: Tokyo, Japan, 1985; pp. 158.
26. Emanuel, A.; Olander, D. R. Diffusion Coefficients of Copper Sulfate in Water and Water in n-Butyl Alcohol. *J. Chem. Eng. Data* **1963**, *8*, 31-32.
27. Eversole, W. G.; Kindsvater, H. M.; Peterson, J. D. The Diffusion Coefficient of Cupric Sulfate from 0.0 to 0.35 Molar at 25° C. *J.*

 doi:10.20944/preprints202210.0269.v1

Phys. Chem. **1942**, *3*, 370-375.